



## Afterslip (and only afterslip) following the 2004 Parkfield, California, earthquake

Andrew M. Freed<sup>1</sup>

Received 30 December 2006; revised 19 February 2007; accepted 28 February 2007; published 31 March 2007.

[1] An analysis of the first two years of postseismic surface deformations from GPS reveals that afterslip is the only mechanism significantly contributing to postseismic deformation following the 2004 M6 Parkfield, California earthquake. Finite element modeling shows this event to have been too small to significantly stress the lower crust and upper mantle, thus viscoelastic relaxation did not lead to detectable surface displacements. Similarly, coseismically induced pressure changes in the upper crust were not sufficient to induce a measurable poroelastic response. From 10 days to two years after the Parkfield earthquake, postseismic displacements at all GPS stations experience the same characteristic decay time ( $\sim 2$  weeks). This suggests that only afterslip was activated and the distribution of slip remained unchanged in this time period. Afterslip was found to be broadly distributed in the upper 15 km of the crust and associated with a moment release of much greater magnitude than the coseismic rupture. **Citation:** Freed, A. M. (2007), Afterslip (and only afterslip) following the 2004 Parkfield, California, earthquake, *Geophys. Res. Lett.*, *34*, L06312, doi:10.1029/2006GL029155.

### 1. Introduction

[2] Earthquakes serve as large rock deformation experiments, where coseismic stress changes induce a variety of postseismic responses that provide insight into lithospheric strength (rheology). Postseismic mechanisms include afterslip, where coseismic stress changes drive aseismic slip [e.g., Marone *et al.*, 1991]; poroelastic rebound, where coseismic pressure changes drive fluid flow within the upper crust [e.g., Wang, 2000]; and viscoelastic relaxation, where coseismic stress changes imparted to the hot lower crust and upper mantle cannot be sustained and drive viscoelastic flow [e.g., Thatcher, 1983]. Each of these mechanisms is capable of inducing observable postseismic surface deformations that can then be used to constrain numerical models to help understand the constitutive properties and extent of faulting, the permeability of the crust, the depth of the brittle/ductile transition, and the strength of the lower crust and upper mantle.

[3] The 2004  $M_w = 6$  Parkfield earthquake represents the first time that an event of such small magnitude has been observed postseismically by an array of continuous GPS stations, as previous well observed postseismic responses have been associated with relatively large ( $M_w \geq 7$ ) earth-

quakes. This small moment release constrains coseismic stress loading primarily to the upper crust, perhaps making it unlikely that a viscoelastic response would be initiated, thus enabling a look at the isolated response of the upper crust to an earthquake. An unusually vigorous postseismic response following the Parkfield earthquake was observed within the first few months of the event, exceeding the magnitude of the coseismic displacements [Langbein *et al.*, 2006; Murray and Langbein, 2006]. This is highly unusual when compared to postseismic displacements from larger events, which are usually an order of magnitude smaller. For example, coseismic displacements during the 2002 M7.9 Denali, Alaska earthquake were well over a meter within several km of the fault and more than 30 cm 100 km from the fault [Hreinsdóttir *et al.*, 2006], while postseismic displacements in the first year were less than 10 cm near the fault and less than 3 cm 100 km from the fault [Freed *et al.*, 2006a].

[4] Initial interpretation of the first several months of postseismic deformation following the Parkfield earthquake assumed afterslip to be the only active mechanism [Johanson *et al.*, 2006; Johnson *et al.*, 2006; Langbein *et al.*, 2006; Murray and Langbein, 2006]. Here I use the first 2 years of observed time-series displacements to constrain numerical models of afterslip, poroelastic rebound, and viscoelastic relaxation. I find a consistent transient signal to emerge after the first 10 days that indicates only a single, shallow mechanism is operating, that I interpret as afterslip. This represents the first time that viscoelastic relaxation and poroelastic rebound can be shown to not be participating significantly in a postseismic response, enabling characterization of the spatial and temporal nature of afterslip without concern of trade-offs to other mechanisms.

### 2. Postseismic Constraints

[5] I utilize 22 GPS stations located around the Parkfield region (Figure 1, Table S1 of the auxiliary material),<sup>1</sup> using regionally filtered times-series generated by the USGS (<http://quake.wr.usgs.gov/research/deformation/gps/auto/ParkfieldContin/>). To isolate postseismic transients, displacements due to background interseismic loading were removed. For stations installed years before the 2004 event, prequake velocities were determined from the slope of the time-series displacements prior to the nearby 2003 M6.5 San Simeon earthquake, which caused detectable coseismic offsets in the Parkfield region [Hardebeck *et al.*, 2004; Ji *et al.*, 2004]. Preseismic velocities for stations installed after the Parkfield earthquake were estimated based on interpo-

<sup>1</sup>Department of Earth and Atmospheric Sciences, Purdue University, West Lafayette, Indiana, USA.

<sup>1</sup>Auxiliary material data set is available at <ftp://ftp.agu.org/apend/gl/2006gl029155>. Other auxiliary material files are in the HTML.

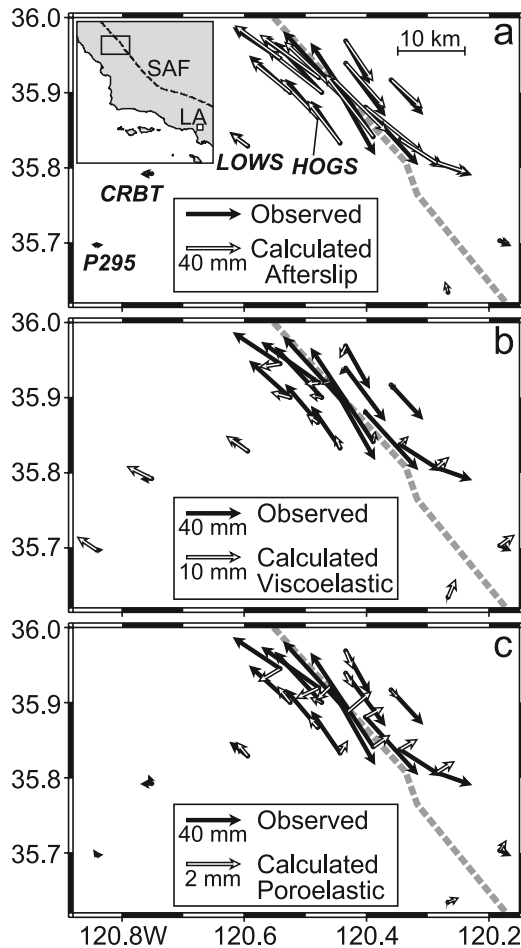


**Figure 1.** Observed surface displacements (black arrows) from 10 days to 2 years after the 2004 Parkfield earthquake and calculated displacements (white arrows) due to (a) afterslip, (b) viscoelastic relaxation, and (c) poroelastic rebound. Observed displacements are based on a logarithmic fit to the time series data. Logarithmic coefficients are listed in Table S1 along with rms misfit. Afterslip displacements are based on an inversion of the GPS displacements. Calculated viscoelastic displacements are from a forward model and represent the maximum possible contribution from relaxation of the lower crust and upper mantle (i.e., complete relaxation of coseismic stresses). Calculated poroelastic displacements are based on a forward model of poroelastic rebound. Displacements are relative to station LCOV (119.058 W/36.360 N). Note the significant differences in velocity scales for the respective displacement sets. The modeled San Andreas fault is shown as a grey dashed line. (inset) The study region (rectangle) relative the San Andreas Fault (SAF) and Los Angeles (LA).

lations from the other prequake velocities using Delaunay triangulation [Shewchuk, 1996]. Figure 2 shows an example of postseismic time-series from 10 days to 2 years for station HOGS. The full set of time-series can be found in Figure S1 of the auxiliary material.

[6] All time-series show a very rapid initial phase of displacement that decays with time, an observation typical of postseismic responses [e.g., Freed *et al.*, 2006b]. To better understand trends in the data, I fit each time-series

using a logarithmic relation of the form  $D = F \ln(1 + \Delta t/\tau)$ , where  $D$  is displacement (mm),  $F$  is a magnification factor (mm),  $\Delta t$  is the time elapsed since the earthquake (years), and  $\tau$  is the decay time (years). I found the time-series to be somewhat variable in the first 10 days before settling down to a consistent pattern of deformation. After 10 days, the postseismic time-series at all stations show transients that can be well fit (rms = 1.6 mm) with a single decay time of 0.04 years ( $\sim 2$  weeks) (Figures 2 and S1). Table S1 lists the magnification factors ( $F$ ) that lead to the minimal misfit of each time-series for this decay time. These magnification factors do not take into account the first 10 days of displacement and the observed and calculated displacements shown in Figures 2 and S1 begin on day 10. Figure S2 shows misfit as a function of decay time assuming a constant decay time for all time-series (an optimal set of magnification factors was determined for each decay time). The best fitting model cannot be substantially improved by using varying decay times between time-series.

[7] The velocity field in the Parkfield region was also influenced by postseismic transients associated with the San Simeon earthquake. Located  $\sim 60$  km away, this thrust event pulled the Parkfield area crust to the southwest, and the region continued drifting in that direction due to post-San Simeon processes. Station P295 was closest to the San Simeon epicenter (23 km away, Figure 1), but was not installed until after the Parkfield earthquake. The next 3 closest stations CRBT (33 km away), LOWS (48 km), and HOGS (59 km) all recorded postseismic transients following the San Simeon earthquake. Having removed background interseismic velocities, I was able to fit post-San Simeon transients at these stations occurring prior to the Parkfield earthquake, finding that the same logarithmic relaxation time as the Parkfield time-series (0.04 years) led to the best-fitting model. Based on these logarithmic fits, I was able to estimate the cumulative contribution of post-San Simeon transients on these stations during the 2 years following the Parkfield earthquake to be  $-2.4$  mm east,  $-4.0$  mm north, for CRBT;  $-1.8$  mm east,  $-2.4$  mm north, for LOWS, and  $-0.9$  mm north,  $-0.7$  mm east for HOGS. All other GPS time-series were influenced by less than 1 mm over the two year time span. I have altered the observed post-Parkfield displacements (Table S1 and Figure 1) by subtracting these small displacements from the post-Parkfield displacements of CRBT and LOWS, ignoring the smaller contributions to the other stations (I did not alter any of the time-series shown in Figures 2 and S1). Based on the location of P295 and the post San Simeon transients recorded at CRBT and LOWS, I estimate a contribution of  $-3.1$  mm east and  $-5.2$  mm north at station P295 during the 2 year post-Parkfield interval.

### 3. Viscoelastic Modeling

[8] Viscoelastic relaxation of a hot lower crust and upper mantle is simulated by developing a 3-D viscoelastic finite element model (FEM) of the Parkfield region, reproducing the coseismic slip distribution, and allowing the lithosphere to relax for 2 years. I used the finite element program I-deas to develop a mesh and perform the coseismic and postseismic calculations, an approach that I have used in several previous postseismic studies [e.g., Freed and Bürgmann,

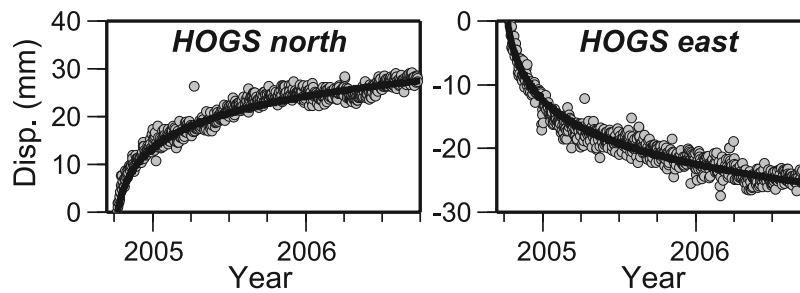


**Figure 2.** Example of continuous GPS observed times-series displacements from 10 days to 2 years after the 2004 Parkfield earthquake (station HOGS) (<http://quake.wr.usgs.gov/research/deformation/gps/auto/ParkfieldContin/>). Black lines show logarithmic fit to the data based on a decay time of 0.04 years and the magnitude factors shown in Table S1. The complete set of times-series and logarithmic fits for all stations can be found in Figure S1.

2004; Freed *et al.*, 2006a]. The FEM utilized 50,000 elements (Figure S3a), with fixed boundary conditions more than 200 km distant and 100 km deep (well beyond the influence of coseismic stress changes). Coseismic slip is simulated by enforcing displacements on a cut within the mesh utilizing the coseismic slip distribution inferred by Langbein *et al.* [2006], based on their joint inversion of trilateration, two-color laser, and GPS data. Though Langbein *et al.* [2006] note that some of the shallow (<5 km) coseismic slip probably occurs on a small fault offset from the main segment, I assumed all of the slip occurred on the SAF using the kinked geometry shown in Figure 1. This model does a reasonable job of matching the GPS observed coseismic surface displacements [Langbein *et al.*, 2006], within the uncertainties of the observations except for a single station very close to the fault (Figure S3b).

[9] We calculate coseismic slip to have induced a shear stress increase at a depth of 20 km (top of lower crust) of only 0.05 MPa, and only 0.01 MPa at the 30-km-deep base of the crust (Figure S3a). This is a relatively small amount of stress with which to drive a postseismic response in the lower crust or upper mantle. Consider, for example, that the  $M_w = 7.9$  2002 Denali, Alaska earthquake induced  $\sim 3.0$  MPa stress increase at 30 km depth [Freed *et al.*, 2006b], a factor of 300 more than the Parkfield event. It is thus quite possible that the Parkfield earthquake was simply not big enough to drive detectable viscoelastic flow in the lower crust and upper mantle. To explore this possibility, I initially chose a small viscosity of  $10^{17}$  Pa s (considered at the bottom of the range usually considered for effective viscosities of the asthenosphere) for both the lower crust (20 to 30 km depth) and upper mantle (30 to 100 km depth). This viscosity leads to complete relaxation of these layers within 2 years, leading to the maximum possible surface displacements that could be driven by a viscoelastic response to the Parkfield earthquake. Figure 1b shows that complete relaxation leads to displacements (white arrows) about an order of magnitude smaller than those observed by GPS (note difference in displacement plotting scales).

[10] In addition to small magnitudes, the deformation pattern calculated to result from viscoelastic flow is significantly different from that observed, with azimuths up to  $90^\circ$  different in the near field. And whereas observed postseismic displacements are largest near the rupture surface and diminish very rapidly with distance, calculated viscoelastic driven surface displacements increase with distance to a maximum at 30–50 km from the fault before

diminishing with further distance. This difference is due to viscoelastic flow occurring much deeper than the mechanism responsible for the observed displacements. The lack of significant observed displacement at station P295, which is about 45 km from the SAF (Figure 1), is evidence that little deformation is occurring in the lower crust or upper mantle (regardless of mechanism), as this is where displacements resulting from such deep-seated shear would be most prominent.

[11] I also worked the calculation assuming that afterslip (discussed subsequently) further loads the lower crust and mantle, which is equivalent to more than doubling stress changes in these regions over the first two year period. This loading was found to be insufficient to drive viscoelastic flow to sufficient levels to induce observable surface displacements ( $<1.5$  mm/yr), in part because of the slowness of such loading. Thus, a component of postseismic viscoelastic relaxation from the 2004 earthquake is likely to never be resolvable in the Parkfield region.

#### 4. Poroelastic Modeling

[12] Coseismic pressure changes upset the equilibrium between pressure gradients and fluids in the shallow crust. In a process referred to as poroelastic rebound, these pressure changes drive fluid flow from this “undrained” condition toward a “drained” condition in which fluid pressure equilibrium is reestablished. These conditions can be described using the same shear modulus with a variation in Poisson’s ratio [Roeloffs, 1996]. Consequently, the drained condition can be modeled using the coseismic calculation with a reduced Poisson’s ratio for the surrounding crust, with rebound displacements found by taking the difference in predicted surface deformation between the drained and undrained models [e.g., Peltzer *et al.*, 1998; Jónsson *et al.*, 2003].

[13] Previous analysis following the 1992 Landers earthquake found that an observed component of postseismic surface deformation could be explained by modeling the drained condition using a reduction in Poisson’s ratio of  $\sim 13\%$  to a depth of 15 km [Peltzer *et al.*, 1998]. In the Parkfield region, the undrained Poisson’s ratio has been inferred from seismic velocities ( $V_p/V_s$  ratios) to be  $\sim 0.27$  [Hauksson, 2000]. Using a similar reduction of Poisson’s ratio with the Parkfield coseismic model (from 0.270 to 0.235) leads to postseismic surface displacements (white arrows in Figure 1c) that are a factor of 40 or more smaller

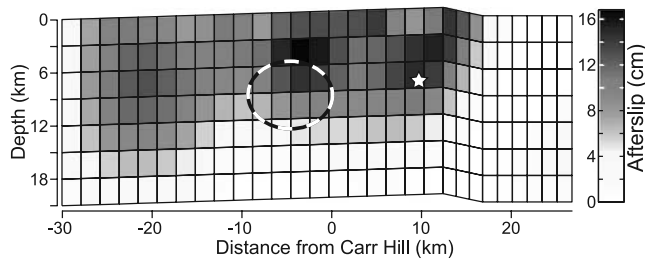


**Figure 3.** Calculated distribution of afterslip based on the inversion of GPS observed cumulative surface displacements for the first 2 years following the 2004 Parkfield earthquake. Black/white circle denotes the region of maximum coseismic slip (order 50 cm). Star denotes the hypocenter.

than those observed (note difference in displacement plotting scales). In addition, many poroelastic displacement azimuths are calculated to be normal to the SAF, while most observed displacement azimuths are parallel.

[14] Poroelastic rebound may have occurred following the Parkfield earthquake, as the crust has a significant fluid content, but coseismic pressure changes appear to have been too small to drive an observable rebound signal at the available GPS sites. This is true even if I double the reduction in Poisson's ratio used to calculate poroelastic rebound, though such decreases would deviate from typical rock properties observed in the laboratory [Rice and Cleary, 1976]. In addition, previous studies of poroelastic rebound suggest the process should be completed within a matter of months [e.g., Masterlark and Wang, 2002; Jónsson et al., 2003], well within the two-year time frame of the time-series used in this analysis. Thus, it is unlikely that an unforeseen component of poroelastic rebound will emerge in the future.

## 5. Afterslip Modeling

[15] Having ruled out significant contributions of viscoelastic relaxation or poroelastic rebound, it appears that afterslip is the only mechanism significantly contributing to observed postseismic surface deformations following the Parkfield earthquake. I can infer the afterslip distribution by inverting the GPS observations for a dislocation model of distributed slip in an elastic half-space. In this approach, similar to that used in previous Parkfield postseismic studies [Johanson et al., 2006; Langbein et al., 2006; Murray and Langbein, 2006], I calculate optimal strike-slip values on a grid of vertical dislocation elements that minimize the misfit (weighted sum of squared residuals) to the GPS data. Positivity constraints (right-lateral strike-slip only) and Laplacian smoothing are applied to avoid mechanically implausible and overly rough slip distributions.

[16] Cumulative surface displacements from 10 days to 2 years following the Parkfield earthquake can be reasonably explained by the afterslip distribution shown in Figure 3. Note how little slip is inferred to occur below 15 km, consistent with viscoelastic modeling results, which suggested relatively small stress changes below this depth from which to drive postseismic shear. The inferred afterslip leads to calculated surface displacements in reasonable

agreement to those observed (Figure 1a). Afterslip appears to be more distributed throughout the fault than coseismic slip, which tended to be concentrated in the outlined region in Figure 3. Even when I decrease smoothing in the inversion, the distribution remains less localized than coseismic slip, with three prominent patches, one overlapping the coseismic slip region, one 10 km to the south of Carr Hill (near the hypocenter), and one 20 km to the north of Carr Hill.

[17] Though the inferred maximum afterslip of 10–15 cm is much smaller than the inferred maximum coseismic slip (order 50 cm), the greater distribution of afterslip leads to an estimated moment magnitude of  $M_w = 6.3$ , compared to  $M_w = 6.0$  for the coseismic rupture, which amounts to  $\sim 3$  times the energy release. And this does not take into account significant slip that occurred over the first 10 days following the earthquake [Langbein et al., 2006]. Significantly larger postseismic moment release compared to the original rupture is not observed following larger strike-slip events ( $M_w \geq 7$ ), where postseismic displacements are generally an order of magnitude smaller than coseismic displacements. Whether this phenomenon is particular to the Parkfield segment or smaller events in general is difficult to determine, as afterslip distributions have not been inferred for many events of this magnitude. One might surmise that significant afterslip following the Parkfield earthquake is due to the fault being only partially locked, as this segment represents a transition from a fully locked segment to the south to a creeping segment to the north. Much of the afterslip appears to occur in regions that were previously inferred to also creep, though at reduced rates prior to the earthquake [Murray and Langbein, 2006].

[18] The 0.04 year logarithmic decay time is also less than what has generally been inferred from studies of larger events. For example, the afterslip component following the  $M_w = 7.9$  2002 Denali earthquake had an estimated decay time of 0.1 years [Freed et al., 2006a]. This longer decay time could be associated with the Denali earthquake being a bigger event or it could be a misinterpretation of the afterslip component, as there were non-uniqueness issues associated with sorting out afterslip versus viscoelastic components to observed post-Denali surface displacements.

[19] My inferred afterslip distribution following the Parkfield earthquake is similar to other afterslip inferences in terms of it being contained to the upper crust, broadly distributed, and being of the same or larger moment release than coseismic slip [Johanson et al., 2006; Johnson et al., 2006; Langbein et al., 2006; Murray and Langbein, 2006]. However, the details of the slip distribution vary widely between analyses, likely due to differences in the time periods considered (most previous analyses only covered the first 6–8 months or less and included the first 10 days following the earthquake), different geodetic constraints utilized, different modeling assumptions, and the general under-constrained nature of afterslip inversions. For example, I infer a region of afterslip that decays but does not migrate over the 2-year span of this analysis, in contrast to the earlier studies. This uniformity is only true, however, after the first 10 days, which earlier analyses did not consider separately. In addition, the slip distribution suggests concentrations of slip above the regions of highest coseismic slip and the hypocenter, which was not found by

other inversions, though some of those inversions inferred higher afterslip to the sides of the coseismic slip patch [Langbein *et al.*, 2006; Murray and Langbein, 2006]. In general agreement with my results, a forward model based on a stress driven rate-and-state friction did find the first 9 months of cumulative surface displacements to be explained by afterslip concentrated just above the region of maximum coseismic slip and the hypocenter [Johnson *et al.*, 2006].

## 6. Summary

[20] Geodetically observed postseismic surface displacements in the 2 years following the 2004  $M_w = 6$  Parkfield earthquake provide a unique opportunity to observe how the central California lithosphere responds to a relatively small earthquake. The response has similarities to larger strike-slip events, such as continued shear motions in the direction of the coseismic and interseismic velocity field, but differs in several important respects: postseismic displacements represent a larger moment release compared to the coseismic rupture, and viscoelastic relaxation and poroelastic rebound provided no significant contributions to observed postseismic displacements, as coseismic stress changes were too small to significantly drive these mechanisms. This leaves afterslip as the only significant active postseismic mechanism, which enables an unfettered look at the behavior of this mechanism. An inversion of postseismic displacements suggest that afterslip is widely distributed along the Parkfield segment of the SAF, with some slip concentrations located near the hypocenter and the region of highest coseismic slip. Postseismic displacements also suggest that the distribution of afterslip remains unaltered with time, and the logarithmic decay rate of 0.04 years ( $\sim 2$  weeks) is much shorter than inferred following larger events.

[21] **Acknowledgments.** I thank Roland Bürgmann for helpful comments on an early draft and two anonymous reviewers who helped me improve the clarity of the manuscript. This work was supported by funds from the Southern California Earthquake Center.

## References

- Freed, A. M., and R. Bürgmann (2004), Evidence of power-law flow in the Mojave Desert mantle, *Nature*, *430*, 548–551.
- Freed, A. M., R. Bürgmann, E. Calais, J. Freymueller, and S. Hreinsdóttir (2006a), Implications of deformation following the 2002 Denali, Alaska, earthquake for postseismic relaxation processes and lithospheric rheology, *J. Geophys. Res.*, *111*, B01401, doi:10.1029/2005JB003894.
- Freed, A. M., R. Bürgmann, E. Calais, and J. Freymueller (2006b), Stress-dependent power-law flow in the upper mantle following the 2002 Denali, Alaska, earthquake, *Earth Planet. Sci. Lett.*, *252*, 481–489.
- Hardebeck, J., et al. (2004), Preliminary report on the 22 December 2003 M 6.5 San Simeon, California earthquake, *Seismol. Res. Lett.*, *75*, 155–172.
- Hauksson, E. (2000), Crustal structure and seismicity distribution adjacent to the Pacific and North America plate boundary in southern California, *J. Geophys. Res.*, *105*, 13,875–13,903.
- Hreinsdóttir, S., J. T. Freymueller, R. Bürgmann, and J. Mitchell (2006), Coseismic deformation of the 2002 Denali Fault earthquake: Insights from GPS measurements, *J. Geophys. Res.*, *111*, B03308, doi:10.1029/2005JB003676.
- Ji, C., K. M. Larson, Y. Tan, K. W. Hudnut, and K. Choi (2004), Slip history of the 2003 San Simeon earthquake constrained by combining 1-Hz GPS, strong motion, and teleseismic data, *Geophys. Res. Lett.*, *31*, L17608, doi:10.1029/2004GL020448.
- Johanson, I. A., E. J. Fielding, F. Rolandone, and R. Bürgmann (2006), Coseismic and postseismic slip of the 2004 Parkfield earthquake from space-geodetic data, *Bull. Seismol. Soc. Am.*, *96*, S269–S282, doi:10.1785/0120050818.
- Johnson, K. M., R. Bürgmann, and K. Larson (2006), Frictional properties on the San Andreas fault near Parkfield, California, inferred from models of afterslip following the 2004 earthquake, *Bull. Seismol. Soc. Am.*, *96*, S321–S338, doi:10.1785/0120050808.
- Jónsson, S., P. Segall, R. Pedersen, and G. Björnsson (2003), Post-earthquake ground movements correlated to pore-pressure transients, *Nature*, *424*, 179–183.
- Langbein, J., J. R. Murray, and H. A. Snyder (2006), Coseismic and initial postseismic deformation from the 2004 Parkfield, California, earthquake, observed by Global Positioning System, electronic distance meter, creepmeters, and borehole strainmeters, *Bull. Seismol. Soc. Am.*, *96*, S304–S320, doi:10.1785/0120050823.
- Marone, C. J., C. H. Scholz, and R. Bilham (1991), On the mechanics of earthquake afterslip, *J. Geophys. Res.*, *96*, 8441–8452.
- Masterlark, T., and H. F. Wang (2002), Transient stress-coupling between the 1992 Landers and 1999 Hector Mine, California, earthquakes, *Bull. Seismol. Soc. Am.*, *92*, 1470–1486.
- Murray, J., and J. Langbein (2006), Slip on the San Andreas fault at Parkfield, California, over two earthquake cycles, and the implications for seismic hazard, *Bull. Seismol. Soc. Am.*, *96*, S283–S303, doi:10.1785/0120050820.
- Peltzer, G., P. Rosen, F. Rogez, and K. Hudnut (1998), Poroelastic rebound along the Landers 1992 earthquake surface rupture, *J. Geophys. Res.*, *103*, 30,131–30,145.
- Rice, J. R., and M. P. Cleary (1976), Some basic stress diffusion solutions for fluid-saturated elastic porous-media with compressible constituents, *Rev. Geophys.*, *14*, 227–241.
- Roeloffs, E. (1996), Poroelastic techniques in the study of earthquake-related hydrological phenomena, *Adv. Geophys.*, *37*, 135–195.
- Shewchuk, J. R. (1996), Triangle: Engineering a 2D quality mesh generator and Delaunay triangulator paper presented at First ACM Workshop on Applied Computational Geometry, Assoc. for Comput. Mach., Philadelphia, Pa., 27–28 May.
- Thatcher, W. (1983), Non-linear strain buildup and the earthquake cycle on the San Andreas Fault, *J. Geophys. Res.*, *88*, 5893–5902.
- Wang, H. F. (2000), *Theory of Linear Poroelasticity With Applications to Geomechanics and Hydrogeology*, 276 pp., Princeton Univ. Press, New Jersey, Princeton, N. J.

A. M. Freed, Department of Earth and Atmospheric Sciences, Purdue University, 550 Stadium Mall Drive, West Lafayette, IN 47907, USA. (freed@purdue.edu)